Longitudinal Observation of Border Tissue Configuration During Axial Elongation in Childhood

Yong Woo Kim,[1] Jin Ju Choi,[2] Michael J. A. Girard,[3,4] Jean Martial Mari,[5] Dong Gyu Choi,[2] and Ki Ho Park[1]

[1]Department of Ophthalmology, Seoul National University Hospital, Seoul National University College of Medicine, Seoul, Korea
[2]Department of Ophthalmology, Kangnam Sacred Heart Hospital, Hallym University College of Medicine, Seoul, Korea
[3]Department of Biomedical Engineering, National University of Singapore, Singapore
[4]Singapore Eye Research Institute, Singapore
[5]University of French Polynesia, Tahiti, French Polynesia

Correspondence: Ki Ho Park, Department of Ophthalmology, Seoul National University College of Medicine, 101 Daehak-ro, Jongno-gu, Seoul 03080, Korea; kihopark@snu.ac.kr.
Dong Gyu Choi, Department of Ophthalmology, Kangnam Sacred Heart Hospital, Hallym University College of Medicine, Seoul, Korea, 1, Singil-ro, Yeongdeungpo-gu, Seoul, 07441, Korea; eyechoi@hallym.or.kr.

YWK and JJC contributed equally to this work as first authors.

Purpose. To investigate the change of border tissue configuration during axial elongation in childhood.

Methods. Fifty-four subjects (108 eyes; age range, 29.3–132.5 months) who had undergone a series of swept-source optical coherence tomography scans at intervals of 6 months or longer were classified into stable axial length (AXL) eyes ($n = 55$; AXL change of ≤ 0.36 mm) and elongating AXL eyes ($n = 53$; AXL change of >0.36 mm). The angle between the Bruch's membrane opening (BMO) reference plane and the border tissue of Elschnig was defined as the border tissue angle (BTA). The border tissue angle, BMO distance (BMOD) and minimum rim width (MRW) were measured in the temporal and nasal regions.

Results. During 15.6 ± 7.2 months of follow-up, the AXL significantly increased from 22.8 ± 1.3 mm to 23.3 ± 1.4 mm ($P < 0.001$). Changes of border tissue angle and AXL showed a significant correlation only in the temporal region of elongating AXL eyes ($r = -0.409$; $P = 0.002$), but not in stable AXL eyes. Both BMOD and nasal MRW significantly increased from 1482.5 ± 153.0 to 1506.1 ± 154.6 μm and from 310.6 ± 83.2 to 324.6 ± 95.6 μm, respectively (all Ps < 0.001). The changes of BMOD and nasal MRW showed a significant positive correlation with changes of AXL in elongating AXL eyes but not in stable AXL eyes.

Conclusions. During the axial elongation in childhood, temporal border tissue configuration change, BMO enlargement, and nasal peripapillary tissue elevation showed a significant correlation with changes in the AXL.

Keywords: myopia, axial elongation, lamina cribrosa, border tissue, optical coherence tomography

Myopia induces typical optic nerve head (ONH) changes including optic disc tilt[1,2] and torsion,[3,4] peripapillary atrophy,[5,6] and focal lamina cribrosa (LC) defects.[7,8] These structural changes render accurate ONH-based diagnosis of POAG difficult in myopic eyes.[9] In addition, many epidemiologic studies and meta-analyses have confirmed that myopia increases the risk for POAG.[10–12] Myopic optic disc tilt and torsion is associated with development of a retinal nerve fiber layer defect[13,14] and its subsequent progression in POAG eyes.[15,16] These observations have encouraged clinicians to explore the relationship of myopia with POAG by elucidating the origin of optic disc tilt or torsion and the process of myopic axial elongation in childhood.

Kim et al.[2] assessed serial optic disc images obtained from Korean children (age range, 1–17 years) with myopic shift and demonstrated progressive ONH tilting with the development and/or enlargement of peripapillary atrophy.

Another prospective cohort study from Korea evaluated the deep ONH structure by spectral-domain optical coherence tomography (OCT) in pediatric eyes (age range, 6.7–12.5 years).[17] It demonstrated changes of temporal border tissue from internally oblique to externally oblique but relatively stable Bruch's membrane opening (BMO) distance during axial elongation in myopic eyes. In a subsequent study, the same authors posited nasal horizontal shifting of LC during myopic elongation based on the observation that the angle between the major vascular arcades decreases and the position of the central vascular trunk is dragged to the nasal side.[18] They suggested that the oval shape of optic disc common in myopic eyes originates from nasal LC shift but not tilting itself.

However, the nasal LC shift theory is derived from the assumption that the central vascular trunk is embedded in the LC, not from direct observation of LC insertion or its configuration. The location of the central vascular trunk

might not be an ideal surrogate marker or even evidence for nasal LC shift. Indeed, because the ONH is a three-dimensional (3D) structure, tracking changes in blood vessel or vascular trunk position in a two-dimensional manner cannot grasp the actual phenomenon of ONH change during myopic elongation. Instead, it is necessary to visualize the LC directly to reach any appropriate conclusions on LC shift.

The present study aimed to investigate longitudinal changes of border tissue configuration during axial elongation in childhood, not only in myopic eyes, but also in emmetropic and hyperopic eyes. Swept source OCT (SS-OCT) scanning with image enhancement by the adaptive compensation technique enabled improved visualization of the neural canal opening structure in childhood eyes.[19]

METHODS

The present study was a retrospective longitudinal observational study performed at Kangnam Sacred Heart Hospital after approval by the Institutional Review Board of Hallym University Medical Center (Institutional Review Board No.: 2020-02-024). The participants in the study were subjects enrolled consecutively from April 2016 who had undergone routine SS-OCT optic disc scans for ONH evaluation and met the eligibility criteria. The study followed the tenets of the Declaration of Helsinki (1964), and informed consent was waived owing to the retrospective design and absence of any additional medical intervention.

Study Subjects

For inclusion in the present study, subjects had to be between 3 and 13 years of age and have a series of SS-OCT scans and measurements of axial length (AXL) and cycloplegic refraction obtained at intervals of 6 months or longer. The present study excluded subjects with (1) a best-corrected visual acuity worse than 20/40, (2) evidence of macular or optic nerve abnormality, (3) a history of prematurity or systemic diseases, (4) a history of intraocular or periocular surgery, or (5) poor cooperation for OCT examination.

Each of the subjects underwent complete ophthalmic examinations including measurement of best-corrected visual acuity (converted to logMAR), refraction, and assessment of ocular motility and alignment. The pupils were dilated with cyclopentolate 1% and tropicamide 1% at intervals of 15 minutes, and manual cycloplegic refraction as well as autorefraction by autokeratorefractometry (KR-800A, Topcon, Tokyo, Japan) was assessed 60 minutes after the instillation of the first drop. Based on the refraction, eyes were classified as emmetropia (refraction $< +0.5$ diopters [D] or ≥ -0.5 D), myopia (refraction < -0.5 D), or hyperopia (refraction $\geq +0.5$ D). AXL was measured using partial-coherence interferometry (Lenstar LS-900, Haag-Streit AG, Switzerland). The study subjects were further classified into stable AXL eyes (AXL change of ≤ 0.36 mm) and elongating AXL eyes (AXL change of >0.36 mm), and the criteria were derived from the median AXL change of the entire study population.

SS-OCT Imaging

All eyes were dilated before undergoing SS-OCT (DRI OCT Triton, Topcon) imaging. The 3D disc scans, in 6 mm×6 mm length and 512×256 sizes, were obtained. This protocol captures color fundus photos as well as optic disc scans, allowing for simultaneous evaluation between OCT B-scans and color optic disc photos with the built-in review program (IMAGEnet 6 Version 1.25, Topcon). The retinal nerve fiber layer thickness, rim area, and disc area were automatically measured with the built-in review program (IMAGEnet 6 Version 1.25, Topcon). All of the analyses were performed according to the right-eye orientation. Only high-quality scans with an image quality score of 60 or greater were used for the analysis. Scans with defocus, poor centration, and motion artifacts ($n = 10$ eyes) were excluded from the analysis.

Evaluation of Border Tissue Configuration

In the present study, three horizontal B-scans were selected and analyzed from the center (middle one-third), superior (upper one-third), and inferior (lower one-third) horizontal meridians, and then averaged for the analysis. All of the subsequent measurements were performed with ImageJ software (developed by Wayne Rasband, National Institutes of Health, Bethesda, MD; available at http://imagej.nih.gov/ij/). Serial OCT scans were linked automatically by the "Compare" function of the built-in review program. This function synchronizes the B-scans by detecting the location of blood vessel in the shadowgram and allows for simultaneous evaluation and tracking of serial scan images at the same location. OCT machine scaling was adjusted to a 1:1 micrometer scale before measurement. The obtained scan images were enhanced by the moving average technique available from the built-in review program. The averaged scan images were further enhanced by applying adaptive compensation according to the relevant protocols (contrast exponent = 2; threshold exponent = 6).[20,21]

The two BMOs were connected to define the BMO reference plane. The distance between the two BMO points was defined as the BMO distance (BMOD). The angle between the BMO reference plane and the border tissue of Elschnig was defined as the border tissue angle (BTA). The BTA was measured in the temporal and nasal regions, respectively. The border tissue configuration was classified into three categories of obliqueness: (1) internally oblique, where the border tissue extends internally to the anterior scleral canal opening (ASCO) (BTA of <80°); (2) externally oblique, where the border tissue extends externally to the ASCO (BTA of ≥100°); and (3) nonoblique, where the border tissue is perpendicular relative to the ASCO (80 ≤ BTA < 100).[22] The minimum rim width (MRW), defined as the minimum distance from the BMO to the internal limiting membrane (ILM), was manually measured in both the temporal and nasal regions, respectively. To evaluate the intraobserver and interobserver reproducibility of the BMOD, BTA, and MRW measurements, two observers (Y.W.K. and J.J.C.) blind to the subjects' clinical information performed measurements in 20 randomly selected B-scans. The absolute agreement of a single observer's measurements as well as the two observers were calculated with the intraclass correlation coefficient obtained from a two-way mixed-effect model. The overall methodology for assessment of border tissue and LC configuration is illustrated in Figure 1.
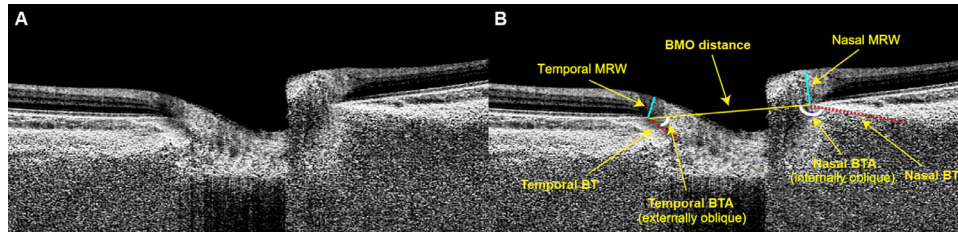
FIGURE 1. Measurements of BMOD, BTA, and MRW. The representative optic disc scan image with adaptive compensation is provided. The two BMOs were connected to define the BMO reference plane. The distance between the two BMO points was defined as the BMOD. The angle between the BMO reference plane and the border tissue of Elschnig (red dotted line) was defined as the BTA. The BTA was measured in the temporal and nasal regions, respectively. The MRW was defined as the minimum distance from the BMO to the internal limiting membrane (ILM) (light blue lines).

Data Analysis

Continuous variables for comparison of initial and final visits were analyzed by the paired t test. Categorical variables were compared using the χ^2 or Fisher's exact test. The false discovery rate was controlled for using the Benjamini–Hochberg method. Except where stated otherwise, the data are presented as mean ± standard deviations, and the level of statistical significance was set at a P value of less than 0.05. All of the statistical analyses were performed with R software (R version 3.6.2., available at: http://www.r-project.org; accessed April 2020).

RESULTS

Subject Demographics

The present study finally included 108 eyes of 54 subjects. The median age of the participants was 80.1 months (age range, 29.3–132.5 months), and all had been followed-up for 15.6 ± 7.2 months (range, 6.3–32.1 months). The medians of baseline refractions and AXL were –0.125 D (range, –10.00 to +7.75 D) and 22.76 mm (range, 19.62–25.17 mm), respectively. The distribution of baseline age, follow-up period, baseline refraction and AXL are provided in Supplementary Figure S1. At baseline, 37 eyes (34.3%) were emmetropic, 35 (32.4%) eyes were myopic, and 36 (33.3%) eyes were hyperopic.

During the study period, the AXL changed significantly from 22.78 ± 1.28 to 23.28 ± 1.42 mm ($P < 0.001$). The median of AXL change was 0.36 mm (range, 0–1.79 mm). Based on this value, the subjects were classified into stable AXL eyes ($n = 55$; AXL change of ≤0.36 mm) and elongating AXL eyes ($n = 53$; AXL change of >0.36 mm). The elongating AXL eyes had significantly older age (88.7 ± 19.8 vs. 67.7 ± 23.6 months; $P < 0.001$) and greater baseline AXL (23.15 ± 1.09 vs. 22.43 ± 1.36 mm; $P = 0.003$) than stable AXL eyes. However, there were no significant differences in follow-up periods, best-corrected visual acuity (in logMAR), refractions, peripapillary retinal nerve fiber layer thickness, rim area, or disc area between the two groups (Table 1). The distribution of AXL and refractions at baseline and final are provided in Supplementary Figure S2.

Border Tissue Configuration Change

The BTA measurements by the two observers showed excellent intraobserver and interobserver reproducibility (Supplementary Table S1). During the study period, the BTA signif-

TABLE 1. Subject Baseline Demographics

	Stable AXL ($n = 55$)	Elongating AXL ($n = 53$)	P Value
FU period, mo	15.4 ± 6.3	15.9 ± 8.0	0.72*
Baseline age, mo	67.7 ± 23.6	88.7 ± 19.8	**<0.001***
Female sex	30 (54.6)	26 (49.1)	0.71†
BCVA (logMAR)	0.01 ± 0.04	0.01 ± 0.02	0.37*
Refraction, D	0.10 ± 3.60	0.35 ± 2.45	0.67*
AXL, mm	22.43 ± 1.36	23.15 ± 1.09	**0.003***
RNFL thickness, μm	109.3 ± 11.2	110.9 ± 9.8	0.42*
Rim area, mm^2	1.50 ± 0.39	1.60 ± 0.39	0.20*
Disc area, mm^2	2.23 ± 0.35	2.36 ± 0.41	0.08*

Values are mean ± standard deviation or number (%).
* Comparison was performed using the Student t test.
† Comparison was performed using the χ^2 test.
Statistically significant P values after the Benjamini–Hochberg procedure are shown in bold.
BCVA, best-corrected visual acuity; FU, follow-up; RNFL, retinal nerve fiber layer.

icantly decreased from 120.0 ± 39.0° to 107.7 ± 43.2° ($P < 0.001$) in the temporal region, and significantly increased from 137.9 ± 31.0° to 139.9 ± 31.6° ($P = 0.001$) in the nasal region. However, in the subgroup analysis, only eyes with elongating AXL (but not eyes with stable AXL) showed a significant BTA change both in the temporal and nasal region (Table 2). The BTA change showed a significant negative correlation with AXL change in the temporal region ($r = -0.555$; $P < 0.001$) and a positive correlation in the nasal region ($r = 0.410$; $P < 0.001$). In the subgroup analysis, elongating AXL eyes showed a significant correlation between

TABLE 2. Change of BTA during Axial Elongation

	Baseline	Final	P Value*	95% CI
Entire population ($n = 108$)				
Temporal	120.0 ± 39.0	107.7 ± 43.2	**<0.001**	–17.0 to 7.8
Nasal	137.9 ± 31.0	139.9 ± 31.6	**0.001**	0.79 to 3.15
Stable AXL ($n = 55$)				
Temporal	120.1 ± 38.4	118.4 ± 39.3	0.15	–4.2 to 0.7
Nasal	131.6 ± 34.2	130.8 ± 34.2	0.24	–2.4 to 0.6
Elongating AXL ($n = 53$)				
Temporal	119.9 ± 40.1	96.5 ± 44.6	**<0.001**	–31.5 to –15.2
Nasal	144.5 ± 26.1	149.4 ± 25.7	**<0.001**	3.4 to 6.4

Values are mean ± standard deviation.
* Comparison was performed using a paired t test. Statistically significant P Values after the Benjamini–Hochberg procedure are shown in bold.

TABLE 3. Change of BMOD During Axial Elongation

	Baseline	Final	*P* Value	95% CI
Entire population ($n = 108$)	1482.5 ± 153.0	1506.1 ± 154.6	**<0.001**	−29.2 to −17.8
Stable AXL ($n = 55$)	1462.4 ± 156.7	1472.3 ± 160.2	**0.002**	−16.2 to −3.7
Elongating AXL ($n = 53$)	1503.5 ± 147.6	1541.1 ± 141.8	**<0.001**	−45.8 to −29.4

Values are mean ± standard deviation.
[*]Comparison was performed using a paired *t* test. Statistically significant *P* values after the Benjamini–Hochberg procedure are shown in bold.

changes of BTA and AXL only in the temporal region ($r = -0.409$; $P = 0.002$), but not in the nasal region ($r = 0.082$; $P = 0.56$). The correlation between changes of temporal BTA and AXL was still significant when adjusted with baseline age of the subjects ($P = 0.005$). In eyes with stable AXL, there was no significant correlation between changes of BTA and AXL, both in the temporal and nasal regions, (all *Ps* > 0.05) (Supplementary Figure S3).

At baseline, the most predominant type of border tissue configuration in the temporal region was internally oblique in hyperopic (86.1%) and emmetropic (70.3%), but was less predominant in myopic eyes (60.0%). Instead, in myopic eyes, the externally oblique border tissue was more predominant (25.7%) than in hyperopic (2.8%) or emmetropic (18.9%) eyes. The externally oblique border tissue in the temporal region had become more prominent at the final visit ($P < 0.001$; Supplementary Table S2). In the nasal region, the most predominant border tissue configuration at baseline was internally oblique in all groups. Myopic eyes had no externally oblique border tissue, whereas 19.4% of hyperopic eyes exhibited an externally oblique border tissue in the nasal region. There was only one case of an externally oblique border tissue in emmetropic eyes at baseline in the nasal region (Supplementary Table S2). The eye-specific changes in BTA and border tissue configurations are animated in Supplementary Video S1.

BMOD and MRW Change

The BMOD and MRW measurements by the two observers showed excellent intraobserver and interobserver reproducibility (Supplementary Table S1). During the study period, the BMOD significantly increased from 1482.5 ± 153.0 µm to 1506.1 ± 154.6 µm ($P < 0.001$). In the subgroup analysis, both elongating and stable AXL eyes showed significant increase of BMOD (mean of the differences, −37.6 [$P < 0.001$] and −9.9 µm [$P = 0.002$], respectively) (Table 3). The increase in BMOD had a significant positive correlation with the increase in AXL ($r = 0.524$; $P < 0.001$). However, this correlation was only significant in elongating AXL eyes ($r = 0.358$; $P = 0.008$), but not in stable AXL eyes ($r = 0.176$; $P = 0.20$) (Supplementary Fig. S4). The correlation between changes of BMOD and AXL were still significant when adjusted with baseline age of the subjects ($P < 0.001$).

During the study period, the nasal MRW significantly increased from 310.6 ± 83.2 µm to 324.6 ± 95.6 µm ($P < 0.001$). However, there was no significant change in the temporal MRW during the same period (Table 4). In the subgroup analysis, the elongating AXL eyes showed a significant increase in nasal MRW (mean of the differences = 21.8 µm; $P < 0.001$), but no change in temporal MRW ($P = 0.11$). The stable AXL eyes did not show any significant changes in neither nasal nor temporal MRW during the same period (Table 4). There was a significant correlation between

TABLE 4. Change of MRW during Axial Elongation

	Baseline	Final	*P*-value[*]	95% CI
Entire population ($n = 108$)				
Temporal	216.7 ± 44.4	214.8 ± 44.7	0.26	−1.4 to 5.2
Nasal	310.6 ± 83.2	324.6 ± 95.6	**<0.001**	7.4 to 20.6
Stable AXL ($n = 55$)				
Temporal	213.2 ± 49.9	213.5 ± 51.0	0.90	−4.6 to 4.0
Nasal	315.4 ± 91.0	321.9 ± 101.0	0.11	−0.9 to 9.1
Elongating AXL ($n = 53$)				
Temporal	220.4 ± 38.1	216.2 ± 37.6	0.16	−1.5 to 8.5
Nasal	305.6 ± 74.8	327.3 ± 90.7	**<0.001**	11.1 to 32.4

Values are mean ± standard deviation.
[*] Comparison was performed using the paired *t* test. Statistically significant *P* values after the Benjamini–Hochberg procedure are shown in bold.

changes of AXL and nasal MRW during the study period ($r = 0.424$; $P < 0.001$). However, this correlation was only significant in elongating AXL eyes ($r = 0.466$; $P < 0.001$) and not in the stable AXL eyes ($P = 0.12$) (Supplementary Fig. S5). The correlation between changes of nasal MRW and AXL were still significant when adjusted with the baseline age of the subjects ($P < 0.001$).

A representative case showing changes in the BTA, BMOD, and MRW during myopic axial elongation is provided in Figure 2. A schematic illustration of longitudinal change of deep ONH structure in myopic eyes is provided in Figure 3.

DISCUSSION

The present study investigated longitudinal changes in the border tissue during axial elongation in childhood, including myopic, emmetropic, and hyperopic eyes. During the study period, the AXL significantly increased with the median value of 0.36 mm. The BTA significantly decreased in the temporal region (i.e., the border tissue changed to externally oblique) and showed a significant negative correlation with AXL change. The BMOD and nasal MRW showed a significant positive correlation with AXL changes especially in eyes with AXL change of more than 0.36 mm.

During myopic axial elongation, the macula moves posteriorly, causing tensile stress to the ONH and neural canal opening. Because the neural canal opening is connected to the superonasal region of the eyeball, the tensile stress to the ONH will be more marked in the temporal region than in the nasal region. This phenomenon is quite analogous to the tensile stress applied to the ONH during adduction of the eyeball. A recent magnetic resonance imaging study demonstrated optic nerve sheath straightening and tethering of the eyeball during adduction.[23] A finite element model study predicted shearing deformation of peripapillary tissues during horizontal eye movements; in
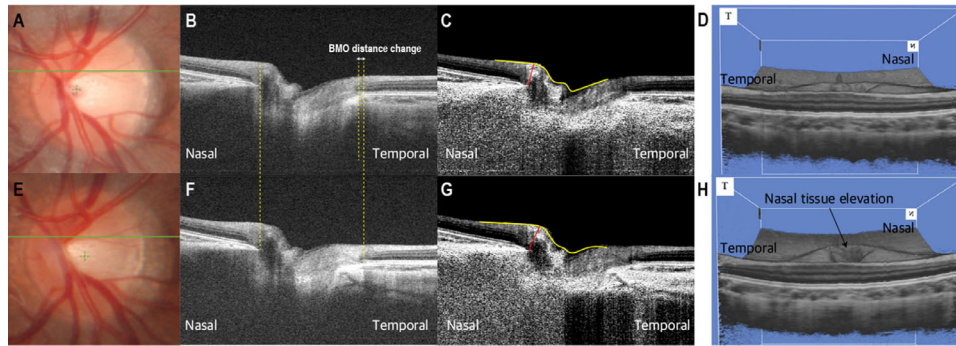
FIGURE 2. Representative case of longitudinal changes of border tissue configuration. Optic disc scan of the left eye of 7-year-old girl at baseline (**A–D**) and final (**E–H**, 18 months later) visits. Enhanced images with adaptive compensation are provided (**C** and **G**). The baseline refraction was –7.25 diopters and changed to –9.125 diopters at the final visit. The AXL increased from 25.05 to 26.14 mm. During the follow-up period, the BMOD increased from 1622 to 1712 μm (**B** and **F**). The temporal BTA decreased from 22.3° to 15.4°, while the nasal BTA changed from 169.4° to 170.8°. The nasal MRW increased from 251 to 268 μm (**C** and **G**). A 3D-rendered OCT image revealed elevation of nasal peripapillary tissues during the follow-up period (**D** and **H**).
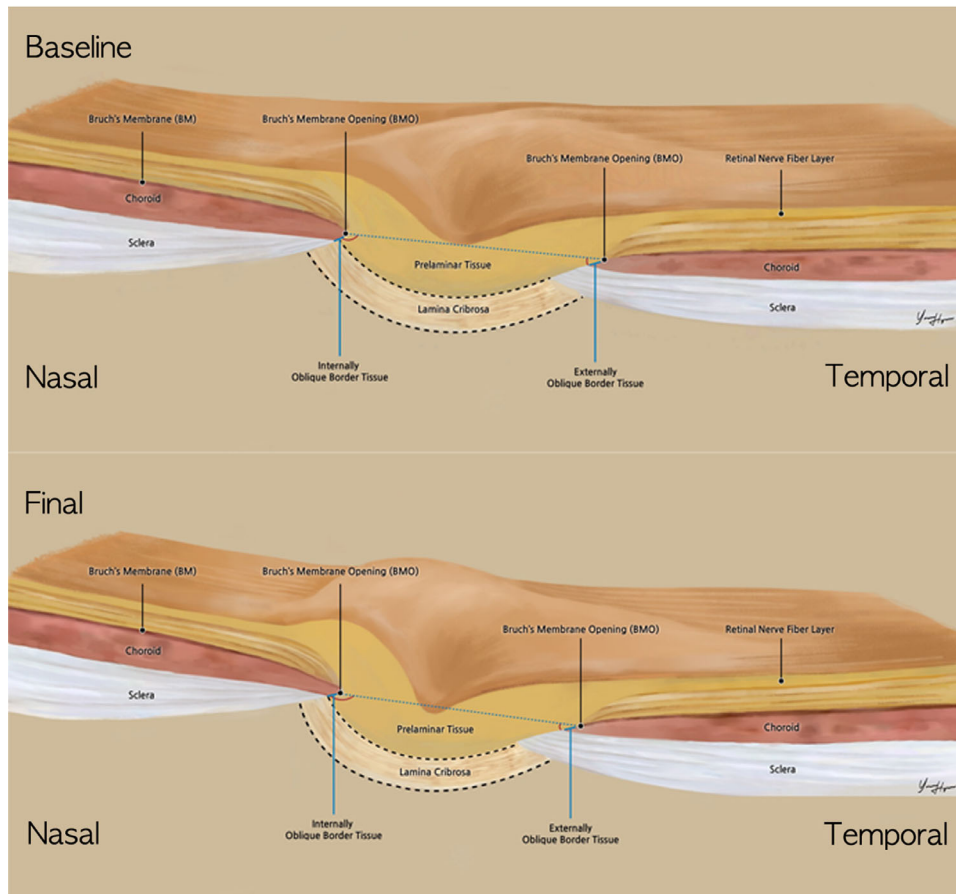

FIGURE 3. Illustration showing longitudinal changes of border tissue configuration in myopic eyes. Note the decreased temporal BTA and relatively stable nasal BTA, and elevation of nasal peripapillary tissue during axial elongation.

adduction, temporal peripapillary tissues are taut posteriorly, whereas nasal peripapillary tissues are elevated anteriorly, and vice versa in abduction.[24] Their subsequent in vivo spectral-domain OCT study exhibited progressive, but transient, temporal ONH tilting and BMO displacement (anterior displacement of nasal BMO and posterior displacement of temporal BMO) during adduction of the eyeball.[25,26] The pattern of ONH change was consistent with the present
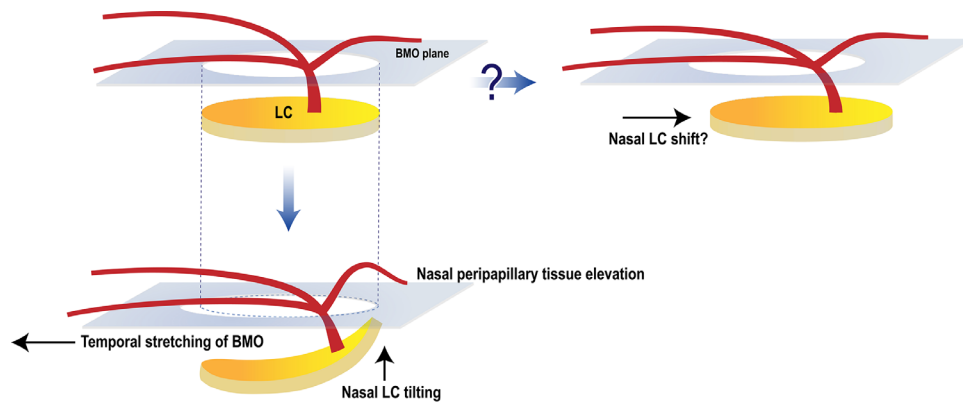
Figure 4. Schematic diagram showing nasal LC tilting during axial elongation in myopic eyes. The previous nasal LC shift theory is depicted in the upper row. The new hypothesis for optic disc tilting in myopic eyes is proposed in the lower row. During axial elongation, the macula moves posteriorly and the BMO stretches to the temporal side (initial BMO size depicted in black dotted line) with elongation of temporal border tissue and configuration change to externally oblique. Owing to the tensile stress in the temporal direction, the nasal neural canal becomes more constricted, and the nasal peripapillary tissue elevates, causing the steeper major vessel and nasal LC to have a pronounced curvature, resulting in the 'lying L' shape and temporal tilt of optic disc.

findings observed during myopic axial elongation. Although myopic axial elongation and adduction of the eyeball are different situations, they share the phenomenon of tensile stress to the temporal region of the ONH.[27] In this sense, it can be postulated that ONH change observed during adduction of the eyeball is analogous to ONH change during myopic axial elongation.

The tensile stress in the temporal ONH during myopic axial elongation can lead to permanent externalization and elongation of the temporal border tissue.[22,28] Recently, Hong et al.[29] investigated the 3D neural canal direction and obliqueness by assessing the ASCO offset relative to BMO. From a cross-sectional observation of 362 healthy eyes, an increase in the AXL was associated with ASCO/BMO offset magnitude, direction, and neural canal obliqueness. In their subsequent study of 69 highly myopic eyes, the BMO and ASCO areas were significantly larger and more elliptical in highly myopic eyes than controls.[30] The neural canal obliqueness was also greater in highly myopic eyes than controls. The present study further demonstrated axial elongation-related changes in the temporal BTA, BMOD, and nasal MRW in myopic eyes. Although the present study differs in that the measurements were made in three, nonradial B-scans per eye and the age range of participants is different, it is quite relevant to the previous two studies in that the BMO can move relative to the underlying ASCO. Considering all of the past and present data together, it can be postulated that, with elongation of the temporal border tissue and its configuration changing to externally oblique, the BMO can be stretched to the temporal side, the nasal neural canal becomes more constricted, and the nasal peripapillary tissue elevates, thereby causing temporal tilt of the optic disc (Fig. 4).

This study has the following limitations. First, owing to its retrospective design, the follow-up interval differed among the subjects. However, there was no significant inter-group difference in the follow-up period. Additionally, the analysis focuses on the effect of AXL changes on outcome parameters, so differences in follow-up periods between subjects may be less affected. Second, the present study protocol did not acquire repeated scans for the outcome parameters so that it is difficult to tell whether the observed changes

exceed the test–retest variability. In this sense, although the changes in the nasal BTA were statistically significant (mean of the differences = –1.96°; $P = 0.001$), it is difficult to tell whether the change was clinically significant in exceeding the test–retest variability. Third, magnification correction can be achieved by DRI Triton OCT by entering the subject's AXL before acquiring the image. However, the acquisition protocol of the present study used a default AXL value of 24.39 mm and did not enter the eye-specific AXL values. To account for the magnification errors, a post hoc adjustment was performed by using the formula of Bennett et al.[31] From this post hoc adjustment, the BMOD still showed significant change during axial elongation in overall study population (mean of the differences = 12.7; $P < 0.001$) and elongating AXL eyes (mean of the differences = 19.5; $P < 0.001$) but not in stable AXL eyes (mean of the differences = 6.2; $P = 0.08$). The nasal MRW also showed significant increase ($P = 0.043$) as well as significant correlation with AXL change ($P = 0.003$). This trend was only significant in elongating AXL eyes and not in stable AXL eyes. However, we decided to keep presenting the original data because this post hoc compensation uses Gullstrand's schematic eye as a model and may introduce errors by oversimplifying the ocular optical system.[32] Fourth, the subjects in the present study were all Koreans, and it is well-known that the biomechanical properties of the ONH can differ by race; thus, the present findings cannot be generalized to other ethnicities.[33,34] Last, the present study included only healthy childhood eyes, and so its findings cannot be extrapolated to glaucoma pathogenesis. To understand the role of myopic ONH changes in glaucoma development, more extensive studies involving patients with myopic glaucoma are needed.

In conclusion, the present study investigated, for the first time, changes of the border tissue configuration during axial elongation in childhood, including myopic, emmetropic, and hyperopic eyes. During this period, the changes in AXL showed a significant correlation with changes of temporal BTA, BMOD, and nasal MRW. The process of myopic axial elongation is a 3D phenomenon and should be monitored as such. The present study broadens the understanding of ONH changes during axial elongation in childhood.

References

1. Samarawickrama C, Mitchell P, Tong L, et al. Myopia-related optic disc and retinal changes in adolescent children from Singapore. *Ophthalmology.* 2011;118:2050–2057.

2. Kim TW, Kim M, Weinreb RN, Woo SJ, Park KH, Hwang JM. Optic disc change with incipient myopia of childhood. *Ophthalmology.* 2012;119:21–26.e21–23.

3. Lee KS, Lee JR, Kook MS. Optic disc torsion presenting as unilateral glaucomatous-appearing visual field defect in young myopic Korean eyes. *Ophthalmology.* 2014;121:1013–1019.

4. Sung MS, Kang YS, Heo H, Park SW. Characteristics of optic disc rotation in myopic eyes. *Ophthalmology.* 2016;123:400–407.

5. Dai Y, Jonas JB, Huang H, Wang M, Sun X. Microstructure of parapapillary atrophy: beta zone and gamma zone. *Invest Ophthalmol Vis Sci.* 2013;54:2013–2018.

6. Vianna JR, Malik R, Danthurebandara VM, et al. Beta and gamma peripapillary atrophy in myopic eyes with and without glaucoma. *Invest Ophthalmol Vis Sci.* 2016;57:3103–3111.

7. Han JC, Cho SH, Sohn DY, Kee C. The characteristics of lamina cribrosa defects in myopic eyes with and without open-angle glaucoma. *Invest Ophthalmol Vis Sci.* 2016;57:486–494.

8. Sawada Y, Araie M, Ishikawa M, Yoshitomi T. Multiple temporal lamina cribrosa defects in myopic eyes with glaucoma and their association with visual field defects. *Ophthalmology.* 2017;124:1600–1611.

9. Tan NYQ, Sng CCA, Jonas JB, Wong TY, Jansonius NM, Ang M. Glaucoma in myopia: diagnostic dilemmas. *Br J Ophthalmol.* 2019;103:1347–1355.

10. Suzuki Y, Iwase A, Araie M, et al. Risk factors for open-angle glaucoma in a Japanese population: the Tajimi Study. *Ophthalmology.* 2006;113:1613–1617.

11. Marcus MW, de Vries MM, Junoy Montolio FG, Jansonius NM. Myopia as a risk factor for open-angle glaucoma: a systematic review and meta-analysis. *Ophthalmology.* 2011;118:1989–1994.e1982.

12. Kim KE, Kim MJ, Park KH, et al. Prevalence, awareness, and risk factors of primary open-angle glaucoma: Korea National Health and Nutrition Examination Survey 2008-2011. *Ophthalmology.* 2016;123:532–541.

13. Choi JA, Park HY, Shin HY, Park CK. Optic disc tilt direction determines the location of initial glaucomatous damage. *Invest Ophthalmol Vis Sci.* 2014;55:4991–4998.

14. Park HY, Lee K, Park CK. Optic disc torsion direction predicts the location of glaucomatous damage in normal-tension glaucoma patients with myopia. *Ophthalmology.* 2012;119:1844–1851.

15. Sung MS, Kang YS, Heo H, Park SW. Optic disc rotation as a clue for predicting visual field progression in myopic normal-tension glaucoma. *Ophthalmology.* 2016;123:1484–1493.

16. Han JC, Lee EJ, Kim SH, Kee C. Visual Field Progression Pattern Associated With Optic Disc Tilt Morphology in Myopic Open-Angle Glaucoma. *Am J Ophthalmol.* 2016;169:33–45.

17. Kim M, Choung HK, Lee KM, Oh S, Kim SH. Longitudinal changes of optic nerve head and peripapillary structure during childhood myopia progression on OCT: Boramae Myopia Cohort Study Report 1. *Ophthalmology.* 2018;125:1215–1223.

18. Lee KM, Choung HK, Kim M, Oh S, Kim SH. Positional change of optic nerve head vasculature during axial elongation as evidence of lamina cribrosa shifting: Boramae Myopia Cohort Study Report 2. *Ophthalmology.* 2018;125:1224–1233.

19. Girard MJ, Tun TA, Husain R, et al. Lamina cribrosa visibility using optical coherence tomography: comparison of devices and effects of image enhancement techniques. *Invest Ophthalmol Vis Sci.* 2015;56:865–874.

20. Girard MJ, Strouthidis NG, Ethier CR, Mari JM. Shadow removal and contrast enhancement in optical coherence tomography images of the human optic nerve head. *Invest Ophthalmol Vis Sci.* 2011;52:7738–7748.

21. Mari JM, Strouthidis NG, Park SC, Girard MJ. Enhancement of lamina cribrosa visibility in optical coherence tomography images using adaptive compensation. *Invest Ophthalmol Vis Sci.* 2013;54:2238–2247.

22. Reis AS, Sharpe GP, Yang H, Nicolela MT, Burgoyne CF, Chauhan BC. Optic disc margin anatomy in patients with glaucoma and normal controls with spectral domain optical coherence tomography. *Ophthalmology.* 2012;119:738–747.

23. Demer JL. Optic nerve sheath as a novel mechanical load on the globe in ocular duction. *Invest Ophthalmol Vis Sci.* 2016;57:1826–1838.

24. Wang X, Rumpel H, Lim WE, et al. Finite element analysis predicts large optic nerve head strains during horizontal eye movements. *Invest Ophthalmol Vis Sci.* 2016;57:2452–2462.

25. Chang MY, Shin A, Park J, et al. Deformation of optic nerve head and peripapillary tissues by horizontal duction. *Am J Ophthalmol.* 2017;174:85–94.

26. Suh SY, Le A, Shin A, Park J, Demer JL. Progressive deformation of the optic nerve head and peripapillary structures by graded horizontal duction. *Invest Ophthalmol Vis Sci.* 2017;58:5015–5021.

27. Wang X, Beotra MR, Tun TA, et al. In vivo 3-dimensional strain mapping confirms large optic nerve head deformations following horizontal eye movements. *Invest Ophthalmol Vis Sci.* 2016;57:5825–5833.

28. Sawada Y, Araie M, Shibata H, Ishikawa M, Iwata T, Yoshitomi T. Optic disc margin anatomic features in myopic eyes with glaucoma with spectral-domain OCT. *Ophthalmology.* 2018;125:1886–1897.

29. Hong S, Yang H, Gardiner SK, et al. OCT-detected optic nerve head neural canal direction, obliqueness, and minimum cross-sectional area in healthy eyes. *Am J Ophthalmol.* 2019;208:185–205.

30. Jeoung JW, Yang H, Gardiner S, et al. Optical coherence tomography optic nerve head morphology in myopia I: implications of anterior scleral canal opening versus Bruch membrane opening offset. *Am J Ophthalmol.* 2020;218:105–119.

31. Bennett AG, Rudnicka AR, Edgar DF. Improvements on Littmann's method of determining the size of retinal features by fundus photography. *Graefes Arch Clin Exp Ophthalmol.* 1994;232:361–367.

32. Atchison DA, Thibos LN. Optical models of the human eye. *Clin Exp Optom.* 2016;99:99–106.

33. Grytz R, Fazio MA, Libertiaux V, et al. Age- and race-related differences in human scleral material properties. *Invest Ophthalmol Vis Sci.* 2014;55:8163–8172.

34. Tamimi EA, Pyne JD, Muli DK, et al. Racioethnic differences in human posterior scleral and optic nerve stump deformation. *Invest Ophthalmol Vis Sci.* 2017;58:4235–4246.